Arch. Metall. Mater. **65** (2020), 1, 219-227

DOI: 10.24425/amm.2019.131118

K. MECH[1*]

MHD SUPPORTED ELECTROREDUCTION OF FORMATE NICKEL COMPLEXES WITH SIMULTANEOUS INCORPORATION OF TiO_2 PARTICLES

The present work concerns analysis of the possibilities of synthesis of Ni-TiO_2 composite coatings from electrolytes containing formate nickel complexes. A magnetic field was applied as an additional factor enabling modification of properties of the synthesized coatings through its influence on electrode processes. The presented data describes the effect of electrode potential, TiO_2 concentration in the electrolyte as well as the value of the magnetic field induction vector on the deposition rate, composition, current efficiency, structure, surface states and morphology of synthesized coatings. The studies were preceded by thermodynamic analysis of the electrolyte. The obtained results indicated possibilities of synthesis of composites containing up to 0.97 wt. % of TiO_2. Depending on applied electrolysis conditions current efficiency amounted to from 61.2 to 75.1%.

Keywords: electrodeposition, Ni-TiO_2 composites, composite coatings, MHD effect

1. Introduction

Synthesis of Ni-TiO_2 composites due to their numerous potential applications has been intensively studied in many research centers in the world [1-3]. Ni-TiO_2 composites have many other potential applications, including selective methanation of CO [4], selective oxidation of chloronitrobenzene to chloraniline [5], hydrogen generation by photoelectrocatalytic glucose reforming [6], or photoreduction of CO_2 to methane [7]. The properties of electrochemically synthesized Ni-TiO_2 were investigated most widely in terms of their photoelectrochemical properties by de Tacconi et al. [8,9]. Spanou et al. reported that galvanostatically deposited coatings exhibit photo-induced hydrophilicity and may be used as self-cleaning coatings [10]. One of the method of synthesis of these materials is electrodeposition. Mohajeri et al. reported results concerning successful pulse potential deposition of Ni-TiO_2 composites of a wide composition range from a Watts bath [11]. Thiemig and Bund obtained Ni-TiO_2 coatings by galvanostatic deposition from sulfamate baths. The authors also investigated changes in zeta potential with pH indicating high dispersion of TiO_2 nanoparticles in a diluted (10^{-3} M) acidic and alkaline solution [12]. A sulfamate bath was also applied by Stankovic et al. for analysis of the influence of TiO_2 concentration in the electrolyte on the surface properties of deposited the Ni-TiO_2 coatings. The synthesized coatings contained up to ca. 4 wt. % of TiO_2 at a very high concentration of TiO_2 in the electrolyte amounting to 80 g/L [13]. The number of papers devoted to the synthesis of Ni-TiO_2 composites in recent years shows that investigations focused on analysis of effects influencing the transport kinetics in electrochemical aqueous systems containing nickel ions and ceramic particles are still of great importance. The physicochemical properties of electrochemically synthesized composite coatings are strongly dependent on synthesis conditions. The magnetic field may be an additional factor influencing the kinetics of electrode processes and simultaneously the properties of synthesized materials. Literature reports show possibilities of the application of a magnetic field of parallel orientation of the magnetic field induction vector versus the working electrode surface towards the modification of the composition, structure and morphology of alloys and semiconductors [14-18]. The Lorentz force acts on ions as well as diamagnetic particles moving in the electromagnetic field if the lines of the electric field cross the magnetic field ones. If the magnetic field lines are parallel to the electric field lines, then the main role in the transport of species to the electrode surface is played by the paramagnetic force. In electrochemical processes, electric field lines are usually located in a perpendicular direction versus the surface of the working electrode, thus the location of the magnetic field induction vector parallel to the electrode surface generates the

[1] AGH UNIVERSITY OF SCIENCE AND TECHNOLOGY, ACADEMIC CENTRE FOR MATERIALS AND NANOTECHNOLOGY, AL. A. MICKIEWICZA 30, 30-059 KRAKOW, POLAND

* Corresponding author: kmech@agh.edu.pl

largest effect in mass transport resulting from the Lorentz force. The presence of diamagnetic ceramic particles in the electrolyte also results in an electric field disturbance which may result in deposit morphology modification. The interaction between the disturbed electric field and the magnetic field results in the generation of the Lorentz force, which in turn is responsible for the magnetohydrodynamic effect (MHD). As it may be seen in the work of Feng et al., in the near electrode are there are located numerous eddy vortices causing additional convection [19]. The presence of these eddy vortices may positively influence the desorption of gas products formed during cathodic electrode polarization from the electrode surface [20] as well as improve dispersion of particles in the volume of the electrolyte. The results of MHD action may be compared to the effect of electrolyte stirring. Additional mixing in turn increases the gradient of electrochemically active species and reduces the thickness of the diffusion layer, which may influence deposit grain size [21]. Investigations concerning the effect of the magnetic field on the migration of species are not limited only to aqueous solutions. The positive effect of the increase of magnetic field induction vector (up to 1.2 T) on the incorporation of SiC particles as well on the increase of cathodic current efficiency was reported by Peng et al. for Si reinforced Fe-based coatings [22]. The strong influence of the magnetic field on the morphology of Fe-Si composites was also reported by Long et al. [23]. Sun et al. also analyzed the effect of a strong magnetic field on the migration of diamagnetic particles in molten metal proving that the presence of the MHD influences transport processes not only in aqueous electrolytes [24,25].

The studies performed were focused on the development of a novel synthesis method based on the application the MHD effect generated by an external magnetic field for synthesis of Ni-TiO_2 composite coatings as well as on analysis of the influence of synthesis parameters on the properties of deposited coatings.

2. Experiment details

Electrolytes were prepared by dissolution of analytical grade $NiSO_4$ (Aldrich) and HCOOH (85%, Avantor Materials) in deionized water, then the pH of 4 was adjusted. Colloid electrolytes were prepared by the addition of 0-10 g/L of TiO_2 powder (Evonic P25) which is a mixture of anatase (80%) and rutile (20%).

The electrokinetic potential (ZP) of the TiO_2 was measured using a Malvern Zetasizer NANO ZS (Malvern Instruments Ltd.) apparatus, equipped with a He-Ne (λ = 633 nm) laser. The ZP was determined based on 3 measurements. Before measurement, colloid electrolytes were dispersed in the presence of ultrasounds in 2 h. Measurements were performed at room temperature stabilised for 120 s.

Electrochemical tests were performed with the use of a Bio-Logic SP-200 potentiostat/galvanostat. For electrogravimetric tests, the potentiostat was equipped with a Seiko (QCM922A) electrochemical quartz crystal microbalance (EQCM). In electrogravimetric tests, the WE was gold sputtered quartz crystal (A = 0.25 cm^2). The WE was placed perpendicularly to the cell bottom. The electrolyte volume in electrochemical tests was kept at the same level. Electrodeposition of composites was performed onto a copper sheet (A = 3.14 cm^2). Directly before electrodeposition, the electrodes were etched in a mixture of HNO_3 (96%, Avantor Materials), CH_3COOH (99.5%, Aldrich) and H_3PO_4 (85%, Avantor Materials) of a volume ratio of 1:1:1. As reference electrode, a Leakless Ag/AgCl electrode was applied (0.214 V vs NHE). All electrochemical tests as well as electrodeposition were performed at room temperature. After electrodeposition samples were rinsed with distilled water and dried.

Chemical composition was analysed using a WD-XRF (Wavelength Dispersive X-Ray Fluorescence) Rigaku Primini II spectrofluorimeter. Elemental analysis was performed for A = 3.14 cm^2. During measurement, the sample was rotated.

A Quanta 3D 200i scanning electron microscope was used for characterisation of morphology of electrodeposited composite coating. Due to the high roughness factor, observations were performed at a magnification of 2.5 k.

The XPS analyses were carried out in a PHI Versa Probe II Scanning XPS system using monochromatic Al Kα (1486.6 eV) X-rays focused to a 100 μm spot and scanned over an area of 400 μm × 400 μm. The photoelectron take-off angle was 45° and the pass energy in the analyser was set to 46.95 eV to obtain high energy resolution spectra for the Ti 2p, Ni $2p_{3/2}$, C 1s and O 1s regions. A dual beam charge compensation with 7 eV Ar^+ ions and 1 eV electrons were used to maintain a constant sample surface potential regardless of the sample conductivity. All XPS spectra were charge referenced to non-functionalised, saturated carbon (C-C) C1s peak at 284.8 eV. The operating pressure in the analytical chamber was less than 3×10^{-9} mbar. Deconvolution of spectra was carried out using PHI MultiPak software (v.9.7.0.1). The spectrum background was subtracted using the Shirley method.

Magnetic field was generated by a ER-2505 electromagnet (RadioPAN, Poland) and magnetic field induction vector of B = 1 T was oriented in parallel direction vs working electrode surface.

3. Results and discussion

Fig. 1 presents the results of thermodynamic analysis of a Ni^{2+}-$HCOO^-$-H_2O system performed based on data presented in Tab. 1. The distribution diagrams shown indicate that at a pH of 4 and formate ligands concentration of 1 M, nickel ions are complexed into the form of $[Ni(HCOO)]^+$ (92%) and $[Ni(H_2O)_6]^{2+}$ (8%) complexes. The Ni^{2+}-$HCOO^-$-H_2O-TiO_2 system was also analyzed in terms of the electrokinetic potential of the TiO_2 particles. The measured value amounting to - 4.4 mV indicated the high susceptibility of particles for coagulation.

Fig. 2 presents DPV (Differential Pulse Voltammetry) curves registered at different values of magnetic field induction vector using electrolytes containing TiO_2 particles. At a po-

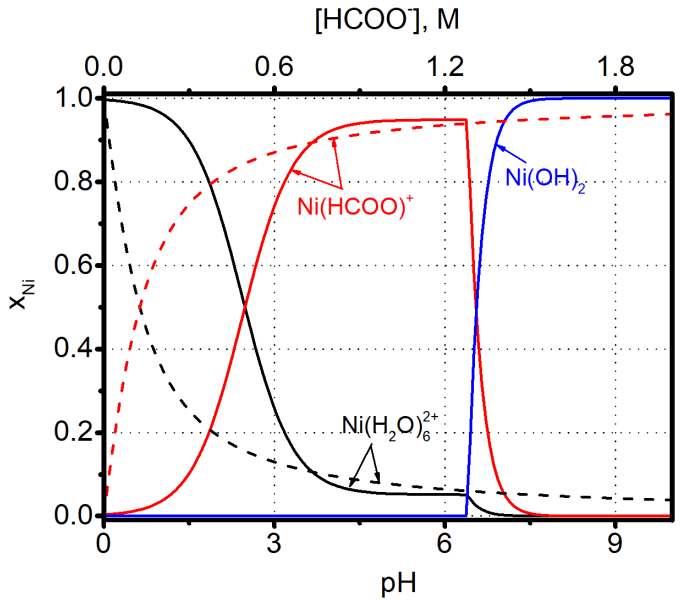

Fig. 1. Distribution diagrams for investigated Ni^{2+}-$HCOO^-$-H_2O system: (solid line – pH dependence, dashed line – ligand concentration dependence)

tential of $E = -0.6$ V voltammograms indicated an increase of cathodic current related to the electroreduction of formate nickel complexes. In TiO_2 free electrolyte, changes in cathodic current density were definitely lower than in the case of electrolytes containing TiO_2 particles. It was observed that at $B = 0$ T, the addition of 5 g/L of TiO_2 to the electrolyte significantly influenced the kinetics of the accompanying hydrogen evolution reaction (HER), causing an increase in cathodic current density (Fig. 2). Further increase of TiO_2 concentration up to 10 g/L did not result in a further increase in cathodic current. In all analyzed

TABLE 1

Reactions considered in calculations of the distribution diagrams with corresponding equilibrium constants ($T = 298$ K)

Ligand	Reaction	logK	Ref.
$HCOO^-$	$H^+ + HCOO^- \rightarrow HCOOH$	3.745	[26]
	$Ni^{2+} + HCOO^- \rightarrow Ni(COOH)^+$	1.31	[27]
H_2O	$Ni^{2+} + 2OH^- \rightarrow Ni(OH)_2$	7.99	[28]
	$Ni^{2+} + 3OH^- \rightarrow Ni(OH)_3^-$	12.3	[29]
	$Ni^{2+} + 4OH^- \rightarrow Ni(OH)_4^{2-}$	9	
	$2Ni^{2+} + OH^- \rightarrow Ni_2(OH)^{3+}$	4.2	
	$4Ni^{2+} + 4OH^- \rightarrow Ni_4(OH)_4^{4+}$	26.1	
	$Ni^{2+} + OH^- \rightarrow Ni(OH)^+$	4.5	
	$Ni^{2+} + 2OH^- \rightarrow Ni(OH)_2(c)$	17.5	
	$Ni^{2+} + H_2O \rightarrow 2H^+ + NiO(c)$	–12.67	[28]

electrolytes, an increase in magnetic field induction vector resulted in an increase in cathodic current density corresponding to peak A (Fig. 2).

In order to determine the influence of the magnetic field on electrode processes, DPV curves were also recorded at different sweep rates in electrolytes containing nickel formate complexes in the presence of magnetic field of different values of magnetic field induction vector (B). Based on current densities corresponding to $E = -0.65$ V, the $i = \zeta(v^{1/2})$ dependence was plotted (Fig. 3). Then diffusion coefficients were estimated with the use of the Berzins-Delahay eq. [30]:

$$i = -3.6733 \cdot 10^5 \cdot z^{\frac{3}{2}} \cdot v^{\frac{1}{2}} \cdot D_j^{\frac{1}{2}} \cdot [j] \qquad (1)$$

where: i – cathodic current density [$A \cdot cm^{-2}$], z – number of electrons consumed in electrode reaction, v – sweep rate [$V \cdot s^{-1}$],

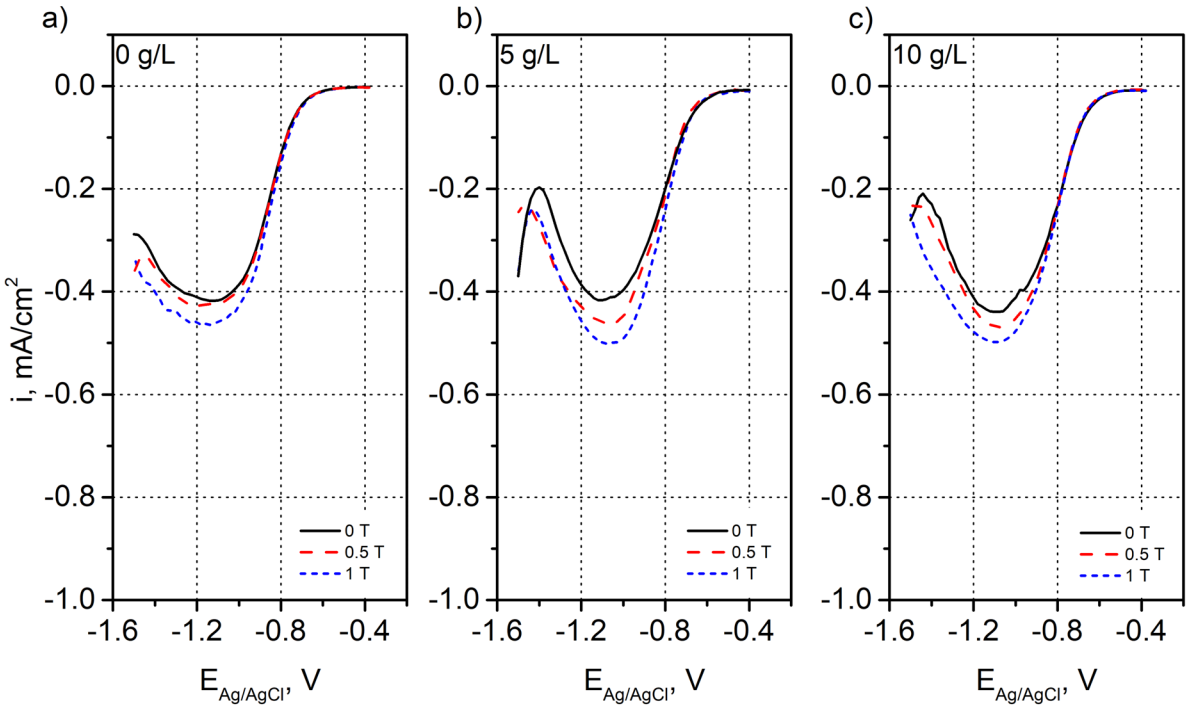

Fig. 2. DPVs registered at different B values and concentration of TiO_2 in the electrolyte of a) 0 g/L, b) 5 g/L and c) 10 g/L ($v = 10$ mV/s)

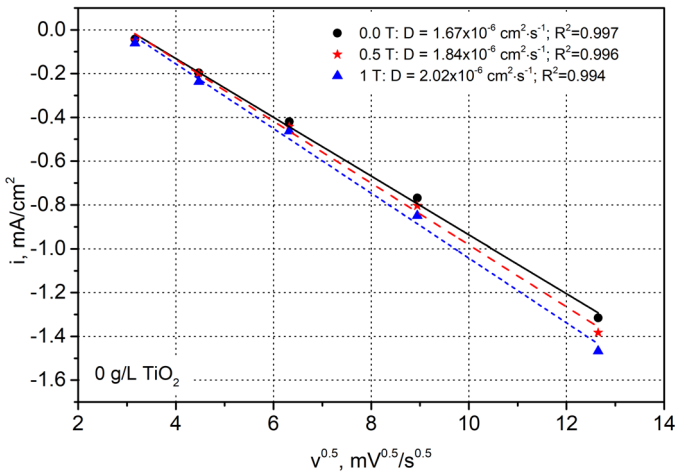

Fig. 3. $i(v^{0.5})$ dependence based on current densities corresponding to $E = -0.65$ V (0 g/L TiO_2)

D_j – diffusion coefficient [$cm^2 \cdot s^{-1}$], and [j] concentration of several complexes in the electrolyte [$mol \cdot cm^{-3}$]. Presence of magnetic field resulted in slight increase of diffusion coefficient from $D = 1.67 \times 10^{-6}$ cm^2/s (0 T) to $D = 2.02 \times 10^{-6}$ cm^2/s (1 T) indicating an increased rate of electrode reactions under magnetic field.

Fig. 4 presents current – time transient curves with corresponding quartz crystal resonator frequency changes. The registered characteristics indicate the significant influence of the magnetic field as well as working electrode potential on the kinetics of composite deposition. The influence of the presence of TiO_2 on electrode kinetics is less visible and is indicated only by a slight increase in cathodic current density. The observed current density values in the system were relatively high. The shape of the recorded current – time transients indicates that composite deposition is accompanied by HER. In the recorded current – time transient curves as well as in some electrogravimetric curves sudden signal changes are visible indicating desorption of hydrogen bubbles from the electrode surface. All analyzed parameters, including working electrode potential, magnetic field induction vector and TiO_2 concentration in the electrolyte, exert a significant impact on the kinetics of reactions taking place at the electrode surface during the synthesis of metallic and composite coatings in the analyzed system.

Fig. 5 presents cyclic voltammograms recorded in electrolytes of different concentrations of TiO_2 particles following the sequence: $E = -0.3$ V → $E = -1.5$ V → $E = 0$ V → $E = -0.3$ V at a sweep rate of $v = 20$ mV/s. Voltammetric tests in Ni^{2+}-$HCOO^-$-H_2O system were performed in an electrochemical window starting from –1.5 V to 0 V, while in the Ni^{2+}-$HCOO^-$-H_2O-TiO_2 system this window was from –1.5 V to 0.5 V. In the potential range close to $E = -1.5$ V in the voltammograms, there are visible perturbations of cathodic current resulting from HER. That is why analysis of the cathodic branches of registered cyclic voltammograms did not allow any conclusions concerning the influence of several electrolysis parameters on the kinetics of electrode processes. Only the clear influence of TiO_2 concentration on an increase in cathodic current density in the HER range was observed. In the case of electrolytes containing TiO_2, the presence of the magnetic field also resulted in an increase in cathodic current especially at the most electronegative potentials. In the insets shown in Fig. 5a and 5c, there are anodic peaks C (for Ni^{2+}-$HCOO^-$-H_2O) or C and D (Ni^{2+}-$HCOO^-$-H_2O-TiO_2) which are related to the oxidation of cathodic deposit formed during the cathodic sweep. The intensity of these peaks is related to the quantity of cathodic deposit formed during the cathodic sweep. It was observed that with an increase in magnetic field induction vector value, the intensity of anodic peaks increased, indicating an increase in the rate of reaction resulting in Ni matrix formation. These conclusions were confirmed by recorded changes in gold covered quartz crystal electrode oscillations which indicated that electrode mass changes increased with an increase in magnetic field induction vector value. The observed effect is related to additional mixing causing a reduction of thickness of the diffusion layer and an increase in the gradient of species present in the electrolyte. The magnetic field induced the formation of an eddy which exerted an effect similar to electrolyte stirring and

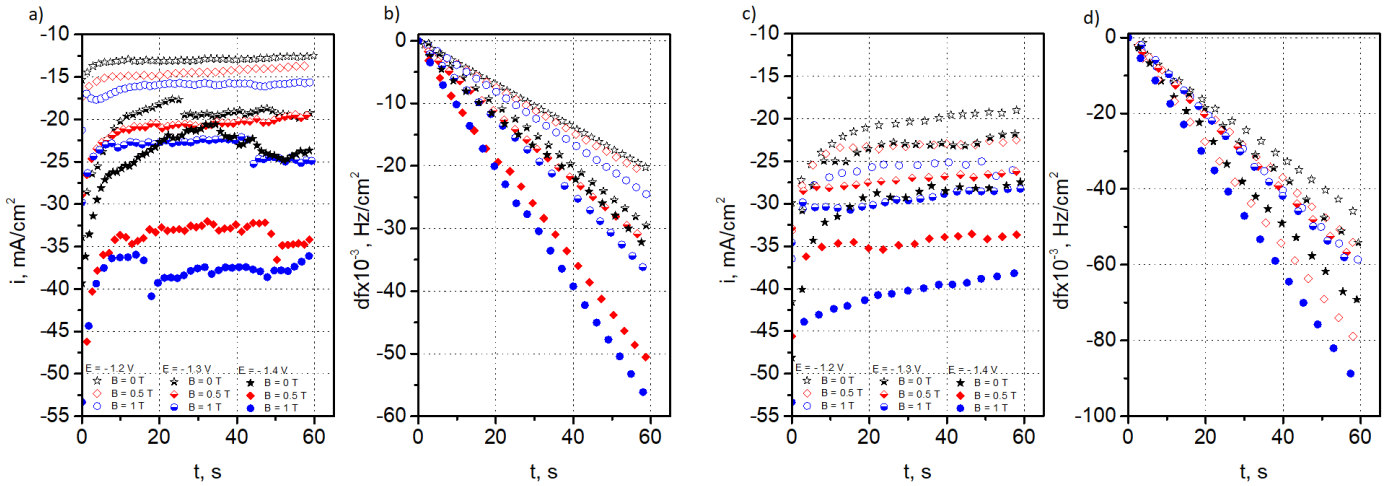

Fig. 4. Current-time transient curves (a, c) with corresponding quartz crystal resonator frequency changes (b, d) recorded during electrolysis performed in electrolytes of different concentration of TiO_2: a, b) 0 g/L, b, d) 10 g/L, different working electrode potentials ($E = -1.2$ V, –1.3 V, –1.4 V), and values of B ($B = 0$, 0.5, 1 T)

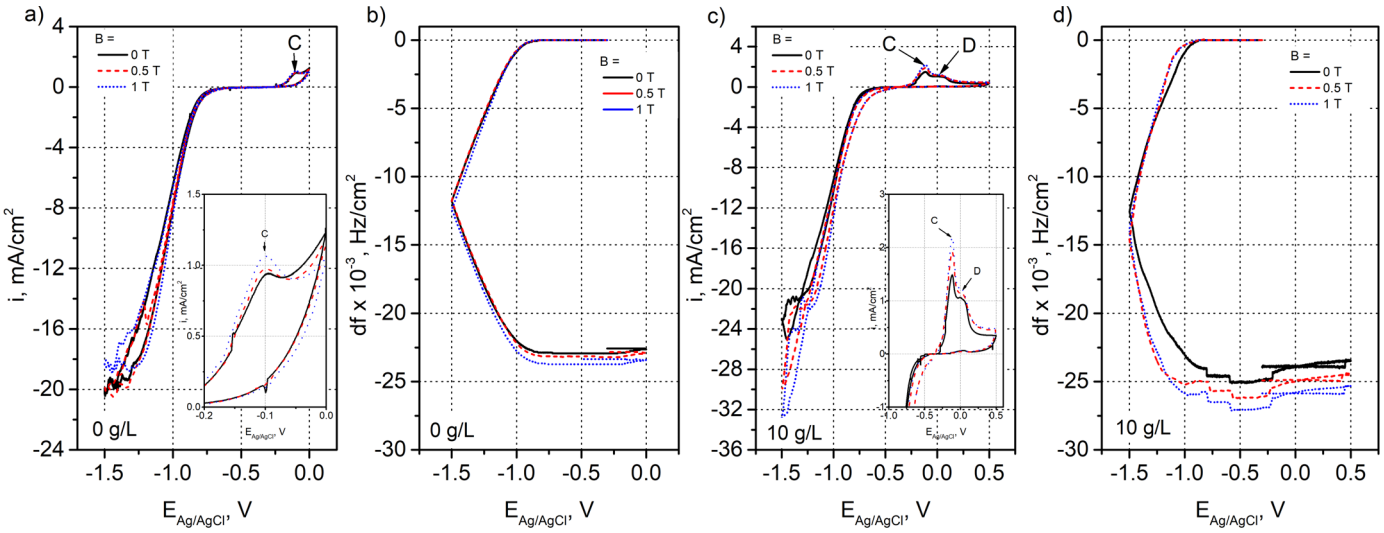

Fig. 5. Cyclic voltammograms with corresponding quartz crystal oscillations frequency changes registered in electrolytes of different concentration of TiO_2 particles: (a, b) 0 g/L, (c, d) 10 g/L and B values (B = 0, 0.5, 1 T) (v = 10 mV/s)

resulted in an increase in the rate of reaction responsible for deposit formation. The peaks C and D seen in the anodic range as well as electrogravimetric curves clearly indicates an increase in deposition rate caused by the presence of the magnetic field.

Fig. 6 presents the composition of synthesized coatings analyzed using the WD-XRF method. The TiO_2 content in composites synthesized in this system without the presence of a magnetic field was relatively low and amounted to from 0.31 wt. % (E = –1.4 V, 5 g/L TiO_2) to 0.65 wt. % (E = –1.2 V, 10 g/L TiO_2). Independently of the working electrode potential, the TiO_2 content in coatings deposited from electrolytes containing 2.5-7.5 g/L TiO_2 was comparable. An increase in TiO_2 concentration to 10 g/L resulted in a slight increase of TiO_2 content in the electrolyte. In the case of coatings synthesized in the presence of a magnetic field, TiO_2 content in coatings synthesized from electrolytes containing 5 g/L and 7.5 g/L TiO_2 was very close. The highest TiO_2 content for coatings synthesized in

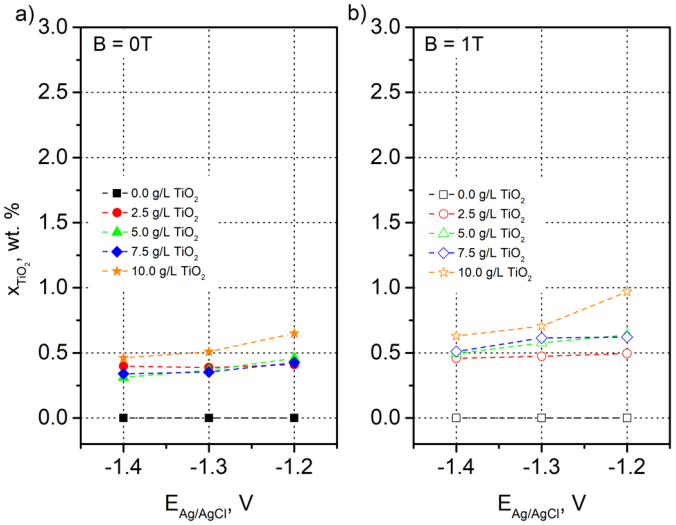

Fig. 6. TiO_2 content in Ni-TiO_2 composite coatings synthesized in Ni^{2+}-$HCOO^-$-H_2O-TiO_2 system a) without external magnetic field, b) at presence of external magnetic field of B = 1 T

the presence of a magnetic field amounting to 0.97 wt. % was observed for an electrolyte containing 10 g/L TiO_2 at a potential of E = –1.2 V.

Fig. 7 presents current – time transient curves recorded during electrodeposition of Ni metal and composite coatings. Curves recorded at B = 0 T show the significant influence of working electrode potential on the kinetics of electrode processes indicating an increase in the rate of electrode reactions with electrode potential decrease. Each further increase of TiO_2 concentration in the electrolyte by 2.5 g/L resulted in an increase in charge quantity by a few coulombs independently of the electrolysis potential applied. The presence of the magnetic field resulted in a significant increase in the rate of electrode reactions, which is confirmed by an increase in the quantity of charge caused by the presence of the magnetic field. Equally visible is the effect of a working electrode decrease (B = 1 T) on an increase in the rate of electrode processes. Apart from synthesis performed using electrolytes containing >5 g/L TiO_2 at E = –1.3 V, an increase in charge quantity related to electrode reactions with an increase of TiO_2 concentration in the electrolyte was noticed. An increase in charge quantity along with electrode potential decrease is typical and is related to significant changes in the kinetics of electrode reactions caused by increased overpotential. The effect of charge increase resulting from the presence of the magnetic field is also clearly visible but results from changes in mass transport processes caused by the magnetic field effect. The nature of the effect and mechanism responsible for the increase in the rate of electrode reactions resulting in coating formation caused by the presence of the magnetic field is different. The observed effect is related to magnetic field induced electrolyte stirring by a formed eddy and an increase in the gradient of species present in the electrolyte.

Tab. 2 presents the charge calculated based on current – time transient curves as well as on differences in electrode mass before and after electrolysis and calculated current efficiency. The current efficiency – electrode potential dependence for

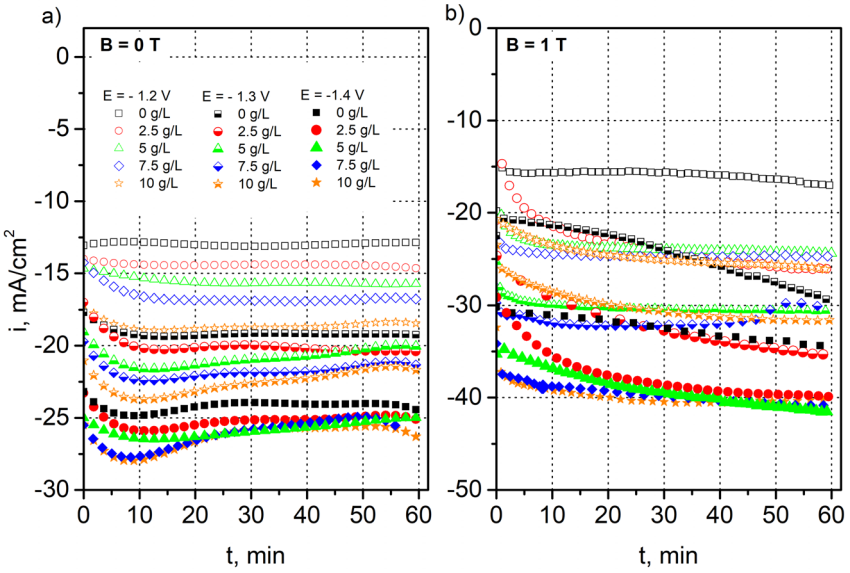

Fig. 7. Current-time transient curves recorded during electrolysis performed a) without external magnetic field, b) at presence of external magnetic field of $B = 1\ T$

different concentrations of TiO_2 and configurations of magnetic field is presented in Fig. 8. Syntheses were performed in Ni^{2+}-$HCOO^-$-H_2O-TiO_2 system of different concentrations of TiO_2 (0; 2.5; 5; 7.5; 10 g/L) at potentials of $E = –1.2$ V, –1.3 V and –1.4 V for magnetic field induction vector values of 0 and 1 T. Electrolysis was conducted for 1h. Independently of the magnetic field configuration, an increase in the current efficiency with electrode potential decrease was observed. Efficiency for synthesis performed at $B = 0\ T$ amounted to from 61.2% for an electrolyte not containing TiO_2 particles to 68.1% for an electrolyte containing 10 g/L TiO_2. In the presence of a magnetic field, both minimal and maximal current efficiency were observed under the same conditions and amounted to from 67.3% to 75.1%.

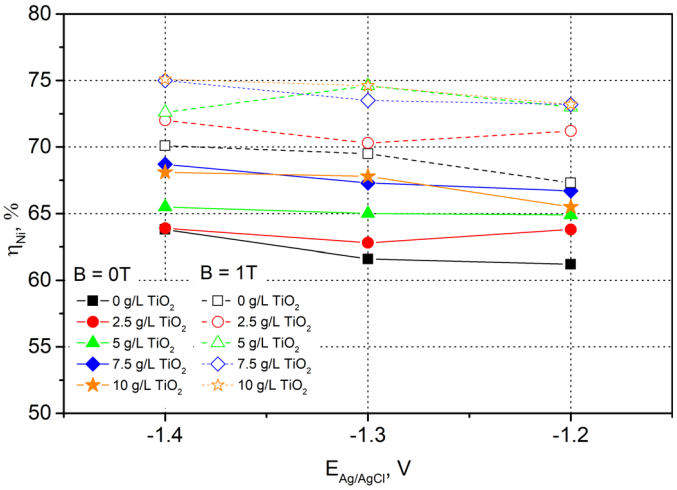

Fig. 8. Current efficiency estimated based on current-time transient curves as well as on changes of the mass of working electrode for deposition of Ni at different electrolysis conditions

Analyses of surface states were performed for coatings of the highest TiO_2 content, deposited without a magnetic field and at $B = 1\ T$. Tab. 3 presents the electrolysis conditions corresponding to synthesis of the analyzed coatings and results of surface elemental analysis performed based on recorded XPS spectra. At the surface of both samples, Ti was detected. In registered XPS spectra there are visible 2p spectral lines of a doublet structure with the main line centered at 458.7 eV, indicating the presence of Ti^{4+} states coming from TiO_2 [31] (Fig. 9). No other Ti states have been detected in the analyzed coatings. At the coatings' surface, large amounts of carbon and oxygen were also detected. The quantities of oxygen and carbon were comparable for both samples and amounted to ca. 37-39 at. % and ca. 31-34 at. % for oxygen and carbon, respectively. These large amounts of carbon

TABLE 2

Charge estimated based on current-time transient curves and based on changes of the mass of working electrode and current efficiency of electrolysis at several conditions

		$B = 0$ T			B = 1 T		
TiO_2, g/L	E, V	q_{ChA}, C	q_{dm}, C	η_{Ni}, %	q_{ChA}, C	q_{dm}, C	η_{Ni}, %
0	–1.2	46.7	28.6	61.2	57.2	38.5	67.3
	–1.3	68.9	42.4	61.6	87.5	60.8	69.5
	–1.4	87.1	55.6	63.8	116.9	81.9	70.1
2.5	–1.2	51.9	33.1	63.8	84.9	60.4	71.2
	–1.3	72.0	45.2	62.8	108.8	76.5	70.3
	–1.4	90.7	58.0	63.9	135.4	97.4	72.0
5.0	–1.2	55.9	36.3	64.9	85.5	62.4	73.0
	–1.3	74.9	48.7	65.0	115.5	86.1	74.6
	–1.4	92.9	60.9	65.5	140.4	102.0	72.6
7.5	–1.2	59.9	39.9	66.7	88.5	64.8	73.2
	–1.3	78.2	52.6	67.3	113.4	83.3	73.5
	–1.4	88.2	60.6	68.7	142.8	107.0	75.0
10	–1.2	67.0	43.9	65.5	88.8	65.0	73.2
	–1.3	81.1	55.0	67.8	108.5	80.9	74.6
	–1.4	94.8	64.6	68.1	143.8	108.0	75.1

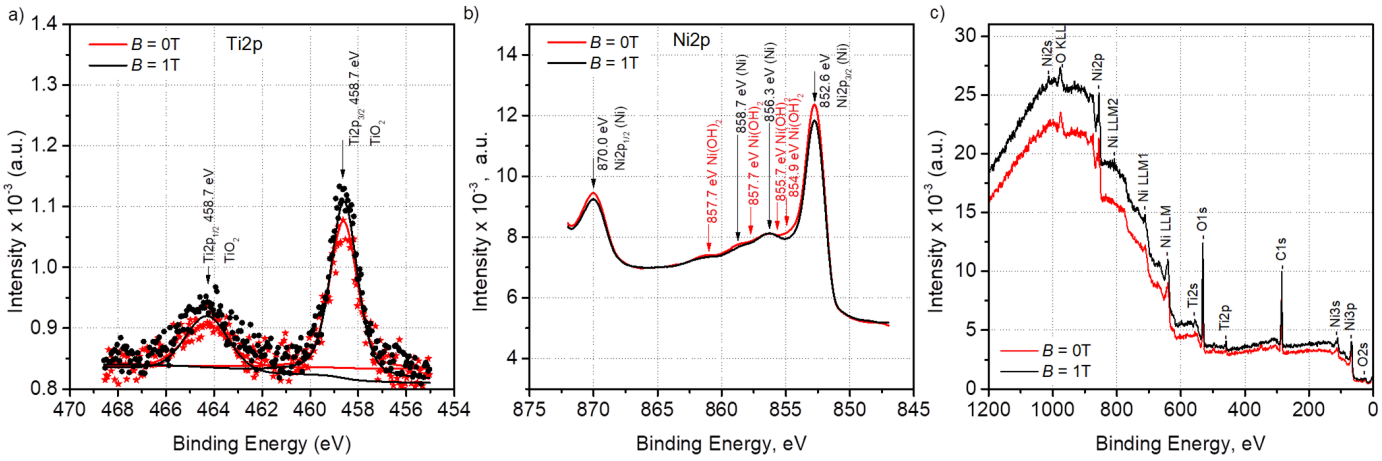

Fig. 9. XPS spectra recorded in Ti2p (a) and Ni2p (b) regimes as well as wide-range spectra (c) for coatings electrodeposited at E = –1.2 V from electrolyte containing 10 g/L TiO_2

and oxygen are probably related to the presence of compounds adsorbed at the surface from the electrolyte as well as from atmospheric air.

TABLE 3

Surface elemental composition (at. %) based on XPS spectra

System	TiO_2, g/L	*E*, V	*B*, T	C	O	Ti	Ni
Ni^{2+}-cit^{3-}-H_2O-TiO_2	10	–1.2	0	38.7	31.0	0.8	29.5
			1	37.2	33.8	1.4	27.7

Fig. 9 presents XPS wide-range spectra recorded for coatings synthesized in a Ni^{2+}-$HCOO^-$-H_2O-TiO_2 system as well as spectra recorded in Ti2p (a) Ni2p (b) regimes. The obtained spectra indicated the presence of $Ti2p_{3/2}$ and $Ti2p_{1/2}$ peaks resulting from TiO_2 present at the coatings' surface, but differences in TiO_2 composition were close to the precision limit, which is why this technique did not supply information concerning the influence of the magnetic field on the surface composition of Ni-TiO_2 coatings.

Fig. 10a presents cross-section with corresponding results of EDS linear scan recorded for Ni-TiO_2 of the highest TiO_2 content (0.97 wt.%). Visible in Fig. 10a, b dark areas corresponding to presence of TiO_2 phase which was confirmed by results of linear (Fig. 10a) and point (Fig. 10b, Tab. 4) EDS analyses. Results indicated also presence of oxygen originating probably from atmospheric air at the sample surface. Elemental composition of coatings corresponding to areas assigned in Fig. 10b was presented in Tab. 4.

TABLE 4

EDS point elemental analysis of areas assigned in Fig. 10b

Point	Ni, at. %	Ti, at. %	O, at. %
1	94.8	1.9	3.2
2	87.3	2.7	10.1
3	99.0	0.3	0.8
4	84.8	3.0	12.2
5	85.6	4.1	10.3
6	100.0	0.0	0.0

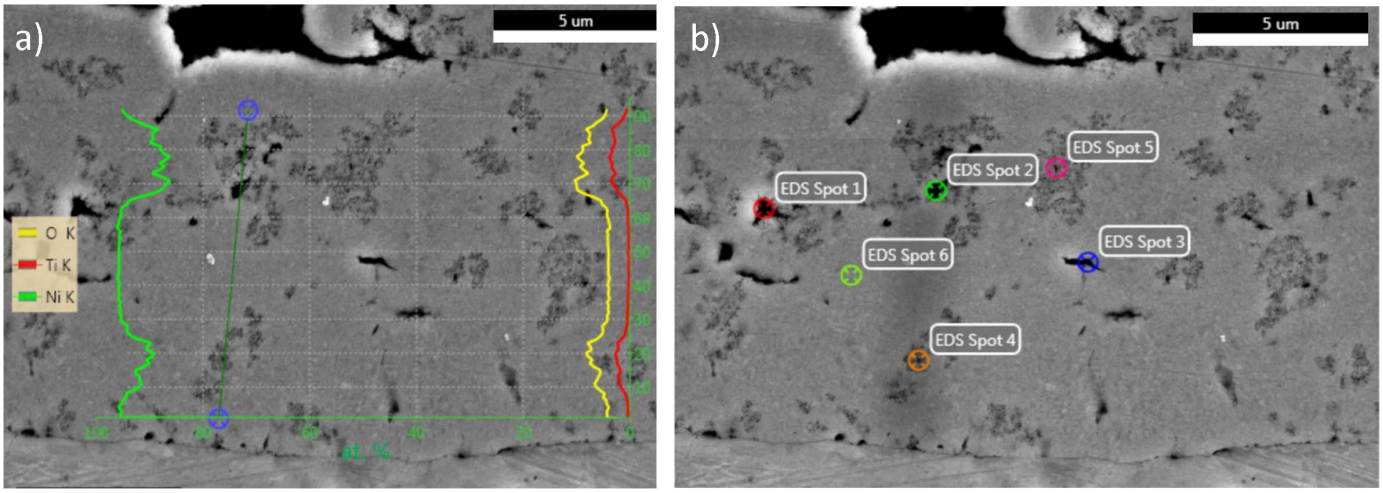

Fig. 10. SEM/EDS linear a) and point b) analyses of cross-section of coating deposited at *E* = –1.2 V from electrolyte containing 10 g/L TiO_2 under magnetic field of *B* = 1 *T*

Fig. 11 presents the morphology of metallic nickel and composite Ni-TiO_2 coatings synthesized in a Ni^{2+}-$HCOO^-$-H_2O-TiO_2 system. The synthesized coatings exhibit a relatively highly developed surface. At the coatings surface, especially in the case of metallic nickel coatings, are visible places in which localized hydrogen evolution took place. A decrease in electrode potential in the case of metallic nickel coatings independently of the presence of TiO_2 in the electrolyte did not significantly influence the surface morphology of the synthesized coatings. It was observed that the presence of the magnetic field resulted in the elimination of pores at the surface of coatings synthesized from TiO_2 free electrolyte.

4. Conclusions

The presented studies indicate the possibilities of synthesis of TiO_2 composite coatings of lower TiO_2 concentration (up

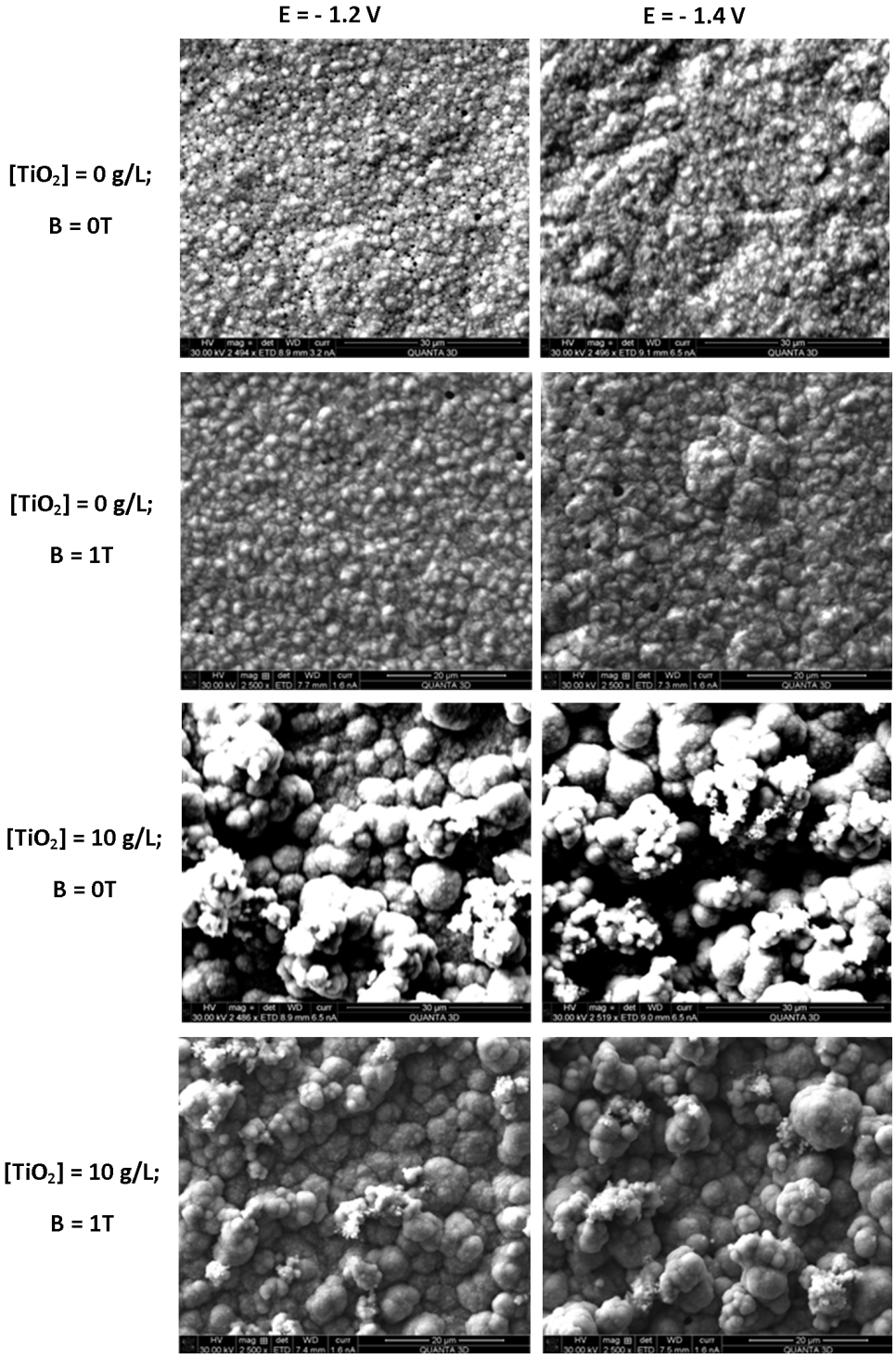

Fig. 11. Morphology of Ni-TiO_2 composites synthesized in Ni_2^+-$HCOO^-$-H_2O and Ni^{2+}-$HCOO^-$-H_2O-TiO_2 systems at different electrolysis conditions

to 0.97 wt. %) in comparison to those deposited from acetate [32] and glycinate [33] baths but at higher current efficiency. The obtained electrochemical results as well as the results of characterization of the obtained coatings show clear evidence of the influence of the MHD effect on the synthesis process and through this on the properties of the deposited coatings. Diffusion coefficients determined at different values of magnetic field induction vector indicate that the magnetic field influence the kinetics of the transport of species to the electrode surface. Current-time transient curves, electrogravimetric studies as well as pores present at the coatings' surface indicate that synthesis is accompanied by hydrogen evolution. It was observed that all parameters, including working electrode potential, TiO_2 concentration in the electrolyte as well as the configuration of the magnetic field, exert a significant impact on the kinetics of electrode processes. Efficiency of Ni matrix electrodeposition amounted to from 61.2 to 75.1% and it was observed that the presence of the magnetic field resulted in an increase in cathodic efficiency by a few %. Registered cyclic voltammograms as well as XPS results indicate the formation of nickel hydroxides and nickel hydrides during the electrodeposition process. The most significant effect on the coatings' surface morphology was exerted by the presence of TiO_2 in the electrolyte. The presence of a magnetic field during the electrodeposition of a nickel coating at $E = -1.2$ V resulted in the elimination of pores formed by localized hydrogen evolution.

Acknowledgements

This work was supported by Polish Ministry of Science and Higher Education under grant IP2015/049974 as well as by Polish National Center of Science under grant 2017/26/D/ST8/00508. K. Mech would like to thank P. Zabinski, M. Marzec and M. Watroba for enabling WD-XRF, XPS and EDS analyses, respectively.

REFERENCES

[1] S.T. Aruna, M. Muniprakash, V.K.W. Grips, J. Appl. Electrochem. **43**, 805-815 (2013).
[2] T. Arunarkavalli, G.U. Kulkarni, G. Sankar, C.N.R. Rao, Catal. Lett. **17**, 29-37 (1993).
[3] W.T. Chen, A. Chan, D. Sun-Waterhouse, J. Catal. **326**, 43-53 (2015).
[4] N. Shimoda, D. Shoji, K. Tani K, Appl. Catal. B-Environ. **174**, 486-495 (2015).
[5] X.C. Meng, H.Y. Cheng, S. Fujita, J. Catal. **269**, 131-139 (2010).
[6] R.M. Mohamed, E.S. Aazam, Chinese J. Catal. **33**, 247-253 (2012).
[7] W.J. Ong, M.M. Gui, S.P. Chai, A.R. Mohamed, RSC Adv. **3**, 4505-4509 (2013).
[8] M. Zhou, N.R. De Tacconi, K. Rajeshwar, J. Electroanal. Chem. **421**, 111-120 (1997).
[9] N.R. De Tacconi, M. Mrkic, K. Rajeshwar, Langmuir **16**, 8426-8431 (2000).
[10] S. Spanou, A.I. Kontos, A. Siokou, A.G. Kontos, N. Vaenas, P. Falaras, E.A. Pavlatou, Electrochim. Acta **105**, 324-332 (2013).
[11] S. Mohajeri, A. Dolati, M. Ghorbani, Surf. Coat. Tech. **262**, 173-183 (2015).
[12] D. Thiemig, A. Bund, Surf. Coat. Tech. **202**, 2976-2984 (2008).
[13] V. Stanković, M. Gojo, V. Grekulovic, N. Pajkić, T. Cigula, J. Min. Metall. Sect. B Metall. **53** (3) 341-348 (2017).
[14] P. Zabiński, K. Mech, R. Kowalik, Arch. Metall. Mater. **57**, 127-133 (2012).
[15] P. Zabiński, K. Mech, R. Kowalik, Electrochim. Acta **104**, 542-548 (2013).
[16] R. Kowalik, K. Mech, D. Kutyla, T. Tokarski, P. Zabinski, Magnetohydrodynamics **51**, 345-351 (2015).
[17] H. Kermoune, A. Levesque, J. Douglad, R. Rehamnia, J.P. Chopart, Ionics **23**, 3565-3570 (2017).
[18] D. Li, Y. Gao, Q. Wang, G. Li, Ch. Wu, A.L. Daltin, J.P. Chopart, J. Electrochem. Soc. **163**, D836-D841 (2016).
[19] Q. Feng, T. Li, Z. Zhang, J. Zhang, M. Liu, J. Jin, Surf. Coat. Tech. **201** (14), 6247-6252 (2007).
[20] J.A. Koza, M. Uhlemann, A. Gebert, L. Schultz, Electrochem. Comm. **10** (9), 1330-1333 (2008).
[21] A. Krause, C. Hamann, M. Uhlemann, A. Gebert, L. Schultz, J. Magn. Magn. Mat. **290-291**, 261-264 (2005).
[22] M. Peng, Y. Zhong, T. Zheng, L. Fan, J. Zhou, W. Ren, Z. Ren, J. Mater. Sci. Technol. **34** (12), 2492-2497 (2018).
[23] Q. Long, Y.B. Zhong, H. Wang, T.X. Zheng, J.F. Zhou, Z.M. Ren, Int. J. Min. Met. Mater. **21** (12), 1175-1186 (2014).
[24] Z.H.I. Sun, X. Zhang, M. Guo, L. Pandelaers, J. Vleugels, O. Van der Biest, K. Van Reusel, B. Blanpain, J. Colloid. Inter. Sci. **375** (1), 203-212 (2012).
[25] Z. Sun, M. Guo, J. Vleugels, B. Blanpain, O. Van der Biest, J. Appl. Phys. **109** (8), 084917 (2011).
[26] A.E. Martel, R.M. Smith, Critical Stability Constants: First Supplement, Springer (1982).
[27] A.E. Martell, R.M. Smith, Critical stability constants. Plenum Press, New York (1976).
[28] B. Beverskog, I. Puigdomenech, Corr. Sci. **39**, 969-980 (1997).
[29] N.V. Plyasunova, Y. Zhang, M. Muhammed, Hydrometallurgy **48**, 43-63 (1998).
[30] T. Berzins, P. Delahay. J. Am. Chem. Soc. **75**, 555-559 (1953).
[31] C.D. Wagner, A.V. Naumkin, A. Kraut-Vass, NIST Standard Reference Database 20, Version 3.4.
[32] K. Mech, Metall. Mater. Trans. A, **50** (9), 4275-4287 (2019).
[33] K. Mech, Mater. Design **182**, 108055 (2019).